Modelling rock glacier velocity and ice content, Khumbu and Lhotse Valleys, Nepal

Yan Hu[1,2,3], Stephan Harrison[2], Lin Liu[1,3], Joanne Laura Wood[2]

[1]Earth System Science Programme, Faculty of Science, The Chinese University of Hong Kong, Hong Kong SAR, China
5 [2]College of Life and Environmental Sciences, University of Exeter, Penryn, Cornwall, TR10 9EZ, UK
[3]Institute of Environment, Energy and Sustainability, The Chinese University of Hong Kong, The Chinese University of Hong Kong, Hong Kong SAR, China

Correspondence to: Yan Hu (huyan@link.cuhk.edu.hk)

10 **Abstract.** Rock glaciers contain significant amounts of ground ice and serve as important freshwater resources as mountain glaciers melt in response to climate warming. However, current knowledge about ice content in rock glaciers has been acquired mainly from in situ investigations in limited study areas, which hinders a comprehensive understanding of ice storage in rock glaciers situated in remote mountains over local to regional scales. In this study, we develop an empirical rheological model to infer ice content of rock glaciers using readily available input data, including rock glacier planar shape, surface slope angle, active layer thickness, and surface creep rate. The model is calibrated and validated using observational data from the Chilean Andes and Swiss Alps. We apply the model to infer the ice content of five rock glaciers in Khumbu and Lhotse Valleys, north-eastern Nepal. The velocity constraints applied to the model are derived from Interferometric Synthetic Aperture Radar (InSAR) measurements. The inferred volumetric ice fraction in Khumbu and Lhotse Valleys ranges from 71% to 75.3% and water volume equivalents lie between 1.40 to 5.92 million m³ for individual landforms. Considering previous mapping results
20 and extrapolating from our findings to the entire Nepalese Himalaya, the total amount of water stored in rock glaciers could be in the magnitude of 10 billion m³, equivalent to a ratio of 1:17 between rock glacier and glacier reservoirs. Due to the accessibility of the input parameters of the model developed in this study, it is promising to apply the approach to permafrost regions where previous information about ice content of rock glaciers is lacking, and ultimately to estimate the water storage potential of the remotely located rock glaciers.

25 # 1 Introduction

Rock glaciers are valley-floor and valley-side landforms consisting of ice–rock mixtures and are common in all arid and cold mountain regions. Recent research has suggested that they represent significant hydrological resources in areas where glaciers are undergoing recession in the face of climate change (Azócar and Brenning, 2010; Jones et al., 2018a; Munroe, 2018; Rangecroft et al., 2014). The potential hydrological value of rock glaciers, and thus their importance in terms of hydrological

30   research, was first noted by Corte (1976); despite this, research on the role of rock glaciers in maintaining hydrological stores in mountain catchments remains limited.

In regions such as the Himalaya, recent research has argued that rock glaciers might represent the end member of an evolutionary process where some glaciers transition to debris-covered glaciers, a proportion of which will then undergo further transition to rock glaciers (Jones et al., 2019; Knight et al., 2019). This process would be triggered by the paraglacial response

35   of high mountain slopes as glaciers undergo downwasting, which produces rock slope failures and mountainside collapses, increasing the flux of rock debris to glacier surfaces. Depending on the debris cover thickness, this would be expected to limit ice melting and increase the resilience of glaciers to climate change (e.g., Reznichenko et al., 2010).

Recent work (Jones et al., 2021) was the first to show that around 25,000 rock glaciers exist in the Himalayas, covering 3747 km² and containing 51.80 ± 10.36 km³ of water volume equivalent. The comparative importance of rock glacier ice content

40   versus that in glaciers in the region was 1:25, ranging from 1:42 to 1:17 in the Eastern and Central Himalaya and falling to 1:9 in Nepal. Importantly, we expect these existing ratios to reduce significantly as glaciers melt and undergo transitions to rock glaciers; yet the rates of transition from glacier to rock glacier are not understood. We also expect rock glaciers to provide water supplies long after glaciers have melted; in other high arid mountains, such as the Andes, ice-cored rock glaciers have persisted in valleys long after glacier recession (Azócar and Brenning, 2010; Monnier and Kinnard, 2015a). However, there

45   lacks modelling studies to test these postulations and to assess the likelihood of glacier–rock glacier transition and the hydrological implications of this process.

A significant gap in our understanding of the likely future hydrological role of rock glaciers in arid mountains is the absence of quantitative information concerning their ice content. Currently, estimates of ice content in rock glaciers have focused on empirical information from drilling cores and boreholes (Hausmann et al., 2007; Monnier and Kinnard, 2013, 2015a, b; Fukui

50   et al., 2007; Arenson et al., 2002; Berthling et al., 2000; Croce and Milana, 2002; Florentine et al., 2014; Fukui et al., 2008; Guglielmin et al., 2004; Guglielmin et al., 2018; Haeberli et al., 1998; Haeberli et al., 1999; Krainer et al., 2015; Leopold et al., 2011; Steig et al., 1998), and from geophysical surveys (e.g., for reviews see: Hauck, 2013; Kneisel et al., 2008; Scott et al., 1990). However, these approaches are costly, time-consuming and extremely difficult to apply to rock glaciers at high altitudes and in remote mountains. It is therefore desirable to develop alternative approaches to understanding the likely ice

55   content of rock glaciers, especially for regional scale estimates.

Ice content is one factor controlling the movement of rock glaciers by influencing the driving force and the rheological properties of materials which constitute the permafrost core (Arenson and Springman, 2005a; Cicoira et al., 2020), thus it is feasible to infer ice content using rheological modelling and observed kinematic data. Here we adapt an empirical rheological model by integrating rheological properties of rock glaciers derived from laboratory experiments (Arenson and Springman,

60   2005a), and parameterise the rheological model based on the structure and composition data of Las Liebres rock glacier (Monnier and Kinnard, 2015b; Monnier and Kinnard, 2016). We then apply the model to simulate surface velocities of four rock glaciers with known ice content in the Swiss Alps and evaluate the modelling results to determine a suitable parameterisation scheme. Finally, we present results from modelling the kinematic responses of the coherently moving part of

five rock glaciers in the study region of north-eastern Nepal and assess the modelled movement as a proxy for ice content by
using remote sensing-derived downslope velocities as constraints.

2 Study area

Our study area comprises the Khumbu and Lhotse valleys in north-eastern Nepal (Fig. 1a). The glaciers draining Everest and
Lhotse (e.g., Khumbu and Lhotse glaciers) are the highest in the world and have well defined debris-covered snouts. The
tributary valleys contain a variety of rock glaciers and composite landforms where glaciers are transitioning to rock glaciers
(Jones et al., 2019; Knight et al., 2019). There are five rock glaciers in the study area, namely Kala-Patthar, Kongma, Lingten,
Nuptse, and Tobuche (Fig. 1b). The five rock glaciers examined in this study are situated at 4900–5090 m a.s.l., near the
altitudinal boundary of discontinuous permafrost in the region. Previous seismic refraction surveys conducted on active rock
glaciers indicate that the lower limit of permafrost occurrence in this region to be ≈5000–5300 m a.s.l. (Jakob, 1992), which
is consistent with an earlier estimate of 4900 m a.s.l. based on ground temperature measurements (Fujii and Higuchi, 1976).
Meteorological data provided by the Pyramid Observatory Laboratory near Lobuche village on the western side of the Khumbu
Glacier (5050 m a.s.l.) reveal that the dominating climate of this area is the South Asian Summer Monsoon. For the period of
1994–2013, recorded accumulated annual precipitation is 449 mm yr^{-1}, with 90% of the precipitation concentrated during
June–September (Salerno et al., 2015). The mean annual air temperature is –2.4 °C (Salerno et al., 2015).
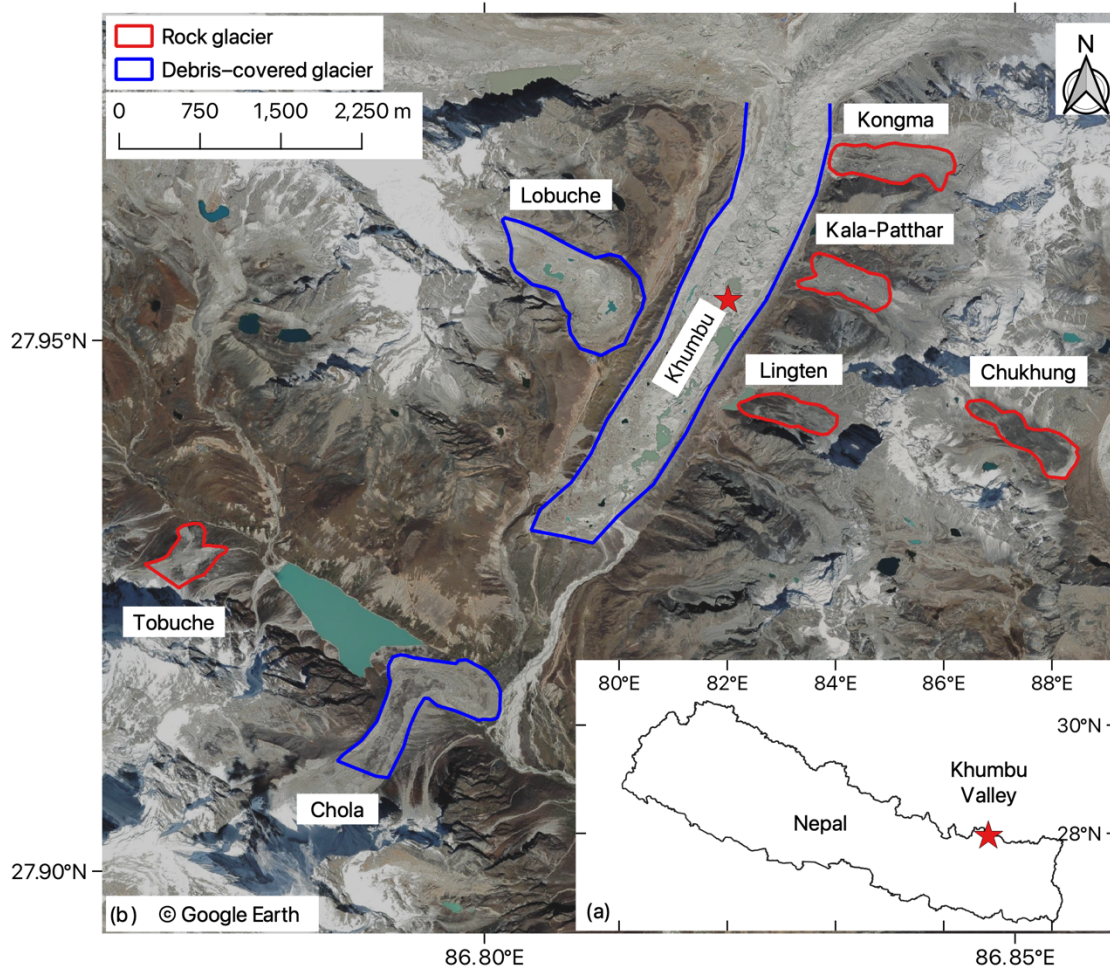
Figure 1: (a) Location of the study site; (b) Google Earth images showing the spatial distribution of the active ice–debris landforms, including rock glaciers (RG) in red outlines and debris-covered glaciers (DCG) in blue boundaries. RGs are delineated based on Google Earth images (Jones et al., 2018b).

3 Methods

Our methods are divided into two parts and detailed in the subsections below. First, we derived surface kinematics of rock glaciers using Interferometric Synthetic Aperture Radar (InSAR; Sect. 3.1). Second, we developed a rheological model for estimating ice content of rock glaciers by using surface velocity as a constraint. Sect. 3.2 describes the model design, calibration, and validation procedures, as well as application of the model.

3.1 Deriving surface kinematics with InSAR

Nineteen L-band ALOS PALSAR images and twenty-one ALOS-2 PALSAR-2 images acquired during 2006–2010 and 2015–2020, respectively, were used to form more than fifty interferograms to measure the surface displacements of the landforms in the study area (Table 1). We selected SAR data to achieve high interferometric coherence by following the criteria such as: (1) short temporal spans (less than 92 days for ALOS pairs and 70 days for ALOS-2 pairs); (2) short perpendicular baselines (smaller than 800 m for ALOS pairs and 400 m for ALOS-2 pairs). We estimated and removed the topographic phase with the 1-arcsec digital elevation models (DEM) produced by the Shuttle Radar Topography Mission (SRTM) (spatial resolution ~30 m). Multi-looking operation and adaptive Goldstein filter (8×8 pixels) were applied to the interferometric processing, which was implemented by the open-source software ISCE version 2.4.2 (available at https://github.com/isce-framework/isce2). The interferograms were unwrapped using the SNAPHU software (Chen and Zebker, 2002). We randomly selected three pixels located at flat and stable ground near each ice–debris landform and averaged their phase values to re-reference the unwrapped phases measured within the landforms. By doing so, atmospheric artefacts including the water vapour delay and ionospheric effects can be effectively removed because these are spatially long-wavelength features and can be assumed as constant within the range of our study objects (Hanssen, 2001).

We then derived the surface velocities along the SAR satellite line-of-sight (LOS) direction from the unwrapped interferograms and projected the LOS velocities to the downslope direction of the landforms. Uncertainties were quantified by considering the error propagation of the InSAR measurements and associated geometry parameters (Hu et al., 2021).

After that, to ensure high data quality, we selected the InSAR observations meeting the following criteria as valid results for further analyses: (1) the pixels showing low coherence (<0.3) are masked out before velocity statistics, and more than 40% of pixels remain after the masking procedure; (2) the mean velocity of the landform is larger than 5 cm yr^{-1}.

Next, we defined and outlined the coherently moving part of the landform by considering the time series of downslope velocity of each pixel acquired during all the observational periods. If the InSAR-measured velocity is higher than 5 cm yr^{-1} in more than half of the periods at a given pixel, it was included into the coherently moving part of the landform.

Finally, we analysed the velocity values of all pixels within the coherently moving part of the landform and selected the mean, median, and maximum values for each observation to characterise the surface kinematics of the landforms.

Table 1. List of ALOS PALSAR and ALOS-2 PALSAR-2 data used in this study.

Satellite	Acquisition interval (days)	Period	Path/frame	Orbit direction	No. of interferograms
ALOS	46	Dec 2007 to Feb 2010	507/540	Ascending	8
ALOS	46	Dec 2007 to Feb 2010	507/550	Ascending	6
ALOS	46	Jun 2007 to Feb 2010	508/540	Ascending	4
ALOS	46	May 2006 to Jul 2006	511/540	Ascending	1
ALOS-2	14	Mar 2015	48/3050	Descending	1
ALOS-2	14	Jun 2015 to Feb 2020	156/550	Ascending	20

3.2 Estimating ice content from a surface-velocity-constrained model

This subsection describes the process of model development. The workflow is illustrated in Fig. 2.
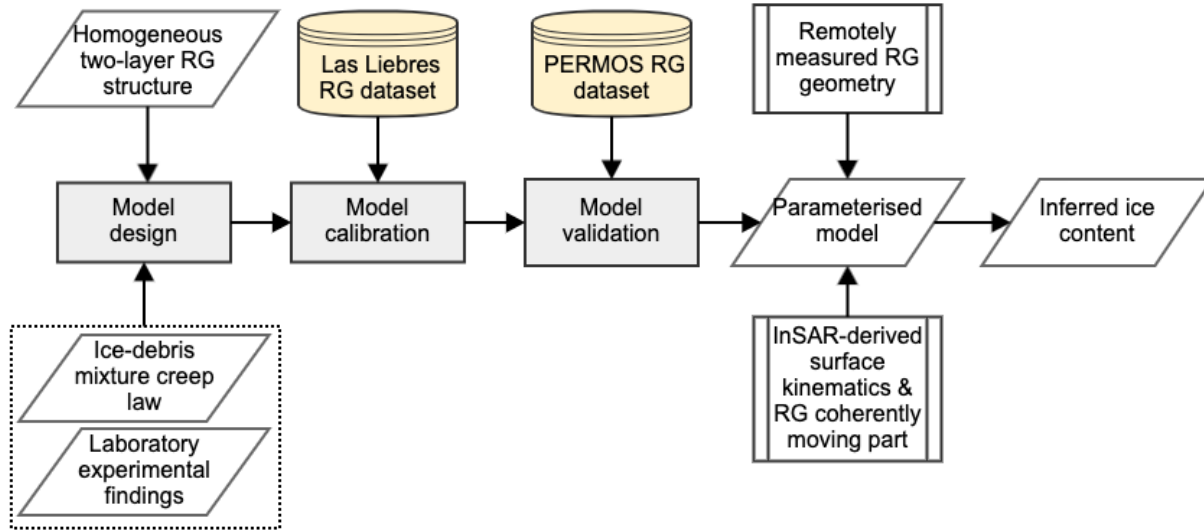
Figure 2: Diagram of the workflow conducted in this study to develop and apply a modelling approach for inferring ice content of
120   **rock glaciers (RG).**

3.2.1 Model design and assumptions

Active rock glaciers creep as a result of two internal processes: plastic deformation of the ice-rich permafrost core, and deformation at the shear horizon at depth (e.g., Arenson et al., 2002; Berthling, 2011; Cicoira et al., 2019b; Haeberli, 2000; Kenner et al., 2019). Many previous modelling studies depict the deformation mechanism of rock glaciers based on Glen's
125   flow law (e.g., Arenson and Springman, 2005a; Cicoira et al., 2020; Whalley and Azizi, 1994), which essentially relates strain rate ($\dot{\varepsilon}$) with effective shear stress (τ) and describes the rheology of ice flow (Glen, 1955):

$$\dot{\varepsilon} = A\tau^n , \tag{1}$$

where A and n are parameters reflecting variations in environmental conditions (mainly including temperature and pressure), material properties (such as composition, structure, and texture), and operating creep mechanisms (e.g., diffusion and
130   dislocation).

In this study, we primarily adopted a creep model of ice–debris mixture, proposed by Moore (2014), based on Glen's flow law:

$$\dot{\varepsilon} = EA[(\tau - \tau_{th})\Gamma]^n , \tag{2}$$

where E is a strain enhancement factor; Γ is a parameter reflecting the strength of the ice–debris mixture, associated with the volumetric debris content (θ_d). When θ_d is less than a critical volumetric debris content (θ_{dc}), the strength of the mixture is
135   governed by interparticle friction, and the value of Γ equals one. Theoretically, θ_{dc} is around 0.52 (Moore, 2014). τ_{th} is a threshold stress imparted by the frictional strength between debris particles, also depending upon the volumetric debris content (θ_d).

Assuming that $\tau_{th} \ll \tau$, $\theta_d < \theta_{dc}$, and $\Gamma = 1$, Eq. 2 can be reduced to the following form (Monnier and Kinnard, 2016):

$$\dot{\varepsilon} = \left(\frac{\tau}{B}\right)^n, \tag{3}$$

140   where B is the effective viscosity and is equal to $\left(\frac{1}{EA}\right)^{-\frac{1}{n}}$.

Following a common setup in glaciology (Cuffey and Paterson, 2010), we consider each rock glacier as a slab with uniform width and thickness and a semi-elliptical cross-section, resting on a bed of constant slope. It consists of two layers: an active layer and a permafrost core. The active layer is a mixture of debris and air, and the permafrost core consists of ice, water, debris and air. Both layers are assumed as homogeneous. Movement of rock glaciers is caused by the steady creep of the

145   permafrost core in the plane parallel to the bed slope. The active layer moves passively along with the inner core, which has been validated by observations (Arenson et al., 2002; Haeberli, 2000). From Eq. 3 and the structure and geometry illustrated in Fig. 3, we have:

$$\frac{du}{dz} = 2\left(\frac{\tau}{B}\right)^n, \tag{4}$$

where $\frac{du}{dz}$ is the velocity derivative relative to the depth z in the permafrost core.

150   At a given depth z, the driving stress τ is imparted, taking into account the loading of the above material and the effect of frictional drag occurring between the lateral margins and surrounding bedrocks, which is represented by a shape factor S_f (Cuffey and Paterson, 2010):

$$\tau(z) = S_f \sin\alpha (\rho_{al} g h_{al} + \rho_{core} g z), \tag{5}$$

where α is the slope angle; g is the gravitational acceleration; ρ_{al} and ρ_{core} are the densities of the active layer and the

155   permafrost core, respectively; h_{al} is the active layer thickness.

The shape factor is expressed as (Oerlemans, 2001):

$$S_f = \frac{\pi}{2} \arctan\left(\frac{W}{2T}\right), \tag{6}$$

where W and T are the width and thickness of the rock glacier, respectively.

The integration of the velocity profile (Eq. 4 and 5) is expressed as:

160    $$\int_0^z du = -2 \left(\frac{S_f g \sin\alpha}{B}\right)^n \int_0^z (\rho_{al} h_{al} + \rho_{core} z)^n dz, \tag{7}$$

$$u(z) = u_s - \frac{2(\rho_{al} h_{al} + \rho_{core} z)^{n+1}}{\rho_{core}(n+1)} \left(\frac{S_f g \sin\alpha}{B}\right)^n, \tag{8}$$

where u_s is the surface velocity as illustrated in Fig. 3. When z is set as the thickness of the ice core (h_{core}) and basal sliding is assumed to be absent, u_s is then expressed as:

$$u_s = \frac{2(\rho_{al} h_{al} + \rho_{core} h_{core})^{n+1}}{\rho_{core}(n+1)} \left(\frac{S_f g \sin\alpha}{B}\right)^n, \tag{9}$$

165   The densities of the active layer (ρ_{al}) and the permafrost core (ρ_{core}) are given as:

$$\rho_{al} = \theta_{d,al} \rho_d + \theta_{a,al} \rho_a, \tag{10}$$

$$\rho_{core} = \theta_{d,core}\rho_d + \theta_{a,core}\rho_a + \theta_{i,core}\rho_i + \theta_{w,core}\rho_w \,, \tag{11}$$

where $\theta_{d,al}$ and $\theta_{a,al}$ are the volumetric contents of debris and air in the active layer, respectively. The volumetric contents of the components in the inner core, namely debris, air, ice and water, are expressed as $\theta_{d,core}$, $\theta_{a,core}$, $\theta_{i,core}$, and $\theta_{w,core}$,

170   respectively. ρ_d, ρ_a, ρ_i, and ρ_w are the densities of debris, air, ice, and water, respectively.

For the flow law exponent (n), we first used an empirical average value as assumed in numerous glaciological studies:

$$n = 3 \,, \tag{12}$$

We also adopted a linear relationship between n and the volumetric ice content ($\theta_{i,core}$) based on laboratory experiments undertaken on borehole samples from two rock glaciers (Arenson and Springman, 2005a):

175   $$n = 3\theta_{i,core} \,, \tag{13}$$
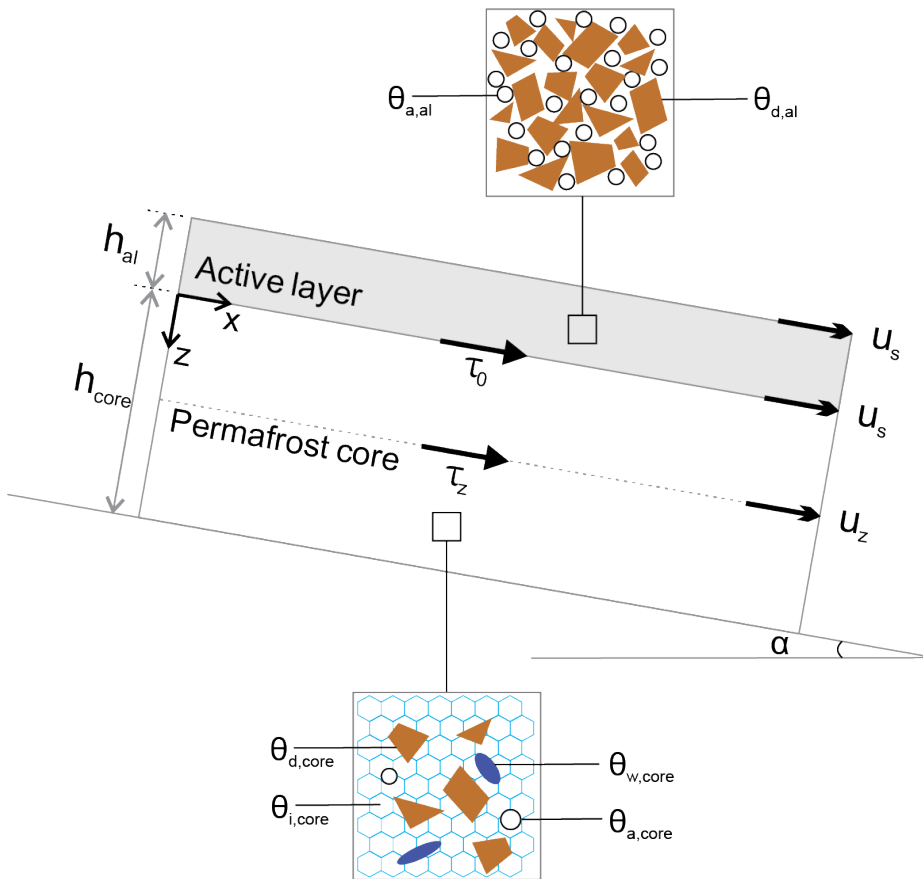
Figure 3: Schematic geometry, structure, stress status, and composition of rock glaciers. The rock glacier consists of a permafrost core underlying the active layer. Parameters involved in the model include surface slope (α), active layer thickness (h_{al}), thickness of permafrost core (h_{core}), driving stress at the base of the active layer (τ_0), driving stress at depth z (τ_z), surface velocity (u_s), velocity at depth z (u_z). $\theta_{d,al}$ and $\theta_{a,al}$ refer to the debris fraction and air fraction of the active layer. $\theta_{d,core}$, $\theta_{i,core}$, $\theta_{w,core}$, and $\theta_{a,core}$ are the fractions of debris, ice, water, and air in the permafrost core, respectively.

3.2.2 Model calibration

Combining Eq. 9–11 with Eq. 12 or 13, we formulated several models depicting the relationship between the surface velocity and properties of rock glaciers, including their composition, structure, and geometry. We then calibrated the models to
185   determine the curve of best fit between the effective viscosity (B) and the volumetric ice content ($\theta_{i,core}$) using observational data of Las Liebres rock glacier in Central Chilean Andes (collected by Monnier and Kinnard, 2015b). This dataset includes information of structure (h_{core} and h_{al}), geometry (α and S_f), and composition ($\theta_{d,core}$, $\theta_{a,core}$, $\theta_{i,core}$, and $\theta_{w,core}$), all of which were derived from Ground Penetrating Radar (GPR) measurements. Surface velocities (u_s) were provided by a Differential Global Positioning System (DGPS) along the central creep line at 14 locations on Las Liebres rock glacier,
190   (detailed in Monnier and Kinnard, 2015b & 2016).

First, we adopted the exponential $B-\theta_{i,core}$ relation estimated by Monnier & Kinnard (2016) with the same dataset and a constant creep parameter n (Eq. 12) (Fig. 4a). Then by integrating the relationship between n and ice content (Eq. 13), we applied both a 2nd-degree polynomial regression model and an exponential regression model to determine the $B-\theta_{i,core}$ relationship (Fig. 4b, c). The polynomial regression model is used to capture the subtle increase in effective viscosity when
195   the ice fraction becomes larger at the ice-rich end. This trend is also depicted in the laboratory experiment conducted by Arenson and Springman (2005a) as a parabolic relationship between the minimum axial creep strain rate and the volumetric ice content. Finally, we obtained three candidate parameterisation schemes expressed as:

$$u_s = \frac{2(\rho_{al}h_{al}+ \rho_{core}h_{core})^4}{\rho_{core}(n+1)}\left(\frac{S_f g \sin \alpha}{35300e^{2.01\theta_{i,core}}}\right)^3 , \tag{14}$$

$$u_s = \frac{2(\rho_{al}h_{al}+ \rho_{core}h_{core})^{3\theta_{i,core}+1}}{\rho_{core}(n+1)}\left(\frac{S_f g \sin \alpha}{7183435\theta_{i,core}^2-9543596\theta_{i,core}+3322637}\right)^{3\theta_{i,core}} , \tag{15}$$

200   $$u_s = \frac{2(\rho_{al}h_{al}+ \rho_{core}h_{core})^{3\theta_{i,core}+1}}{\rho_{core}(n+1)}\left(\frac{S_f g \sin \alpha}{5217905e^{-5.26\theta_{i,core}}}\right)^{3\theta_{i,core}} , \tag{16}$$

For simplicity, the parameterisation scheme proposed in Monnier & Kinnard (2016) is labelled as Scheme 1 (Eq. 14). The parameterisation scheme considering the empirical relation between n and $\theta_{i,core}$ (Eq. 13) and parameterisation scheme derived from the polynomial and exponential relationship between B and $\theta_{i,core}$ are marked as Scheme 2 and Scheme 3 (Eq. 15 and 16), respectively.
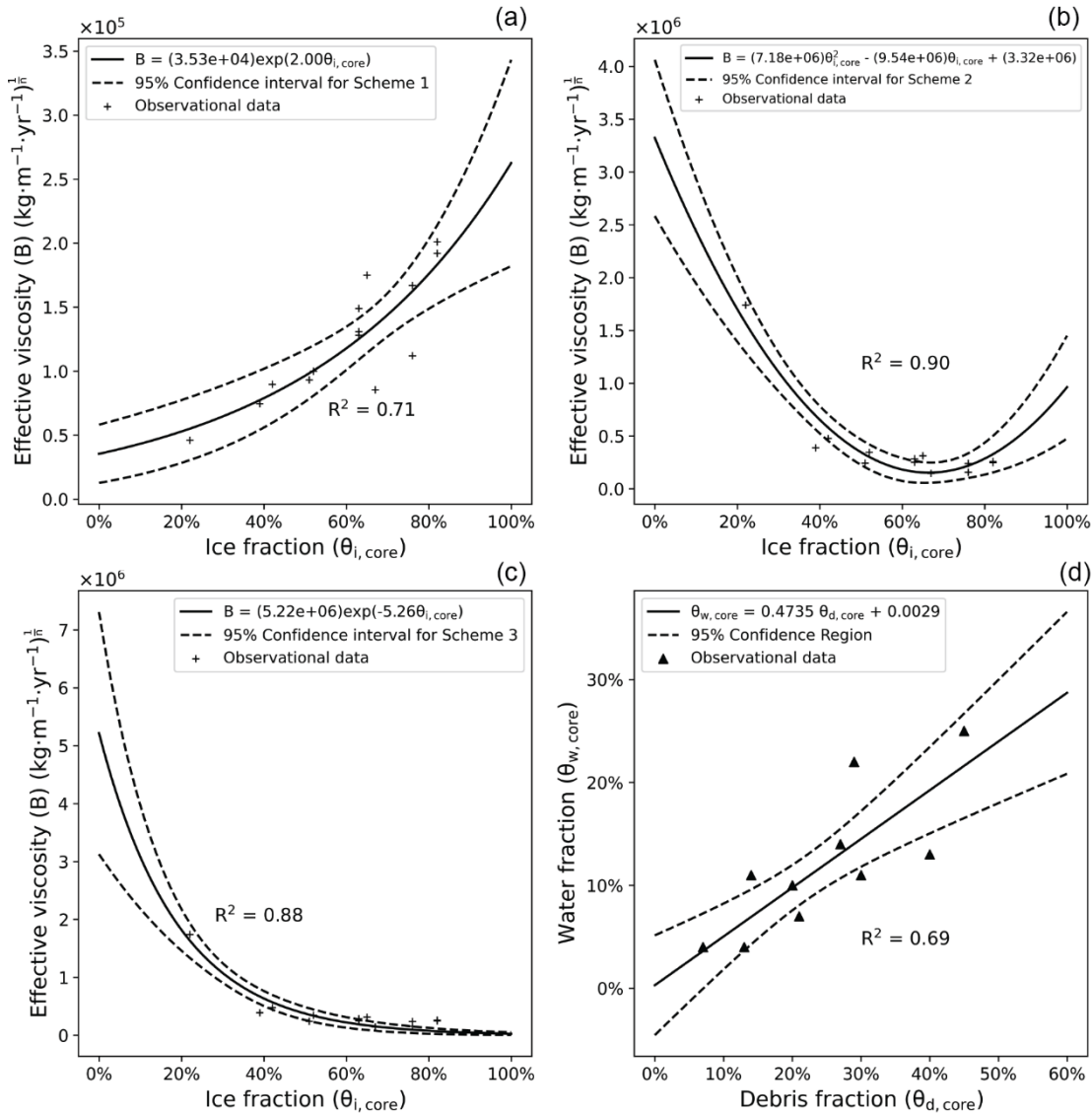
205

Figure 4: (a)–(c) Relationships between the ice fraction ($\theta_{i,core}$) and the effective viscosity (B) estimated from the three regression equations and parameterisation schemes (Eq. 14, 15, and 16, respectively). (d) Relationship between debris fraction ($\theta_{d,core}$) and water fraction ($\theta_{w,core}$). The observational data are derived from the GPR and DGPS measurements in Monnier and Kinnard (2015b & 2016).

3.2.3 Model validation

The three parameterisation schemes (Eq. 14–16) were validated using observational data of four rock glaciers in the Swiss Alps, namely Murtèl-Corvatsch, Gruben, Muragl, and Schafberg (Cicoira et al., 2019a; Arenson et al., 2002; Hoelzle et al., 1998; Barsch et al., 1979). We simulated the surface velocity (u_s) of each rock glacier by varying volumetric ice content

($\theta_{i,core}$) of the permafrost core and inferred its ice fraction by comparing the modelled velocity and the measured velocity
215 from Terrestrial Geodetic Surveys (PERMOS, 2019). We then referred to the previously estimated ice content of the selected
rock glaciers to validate our predicted results.

To derive the input parameters, we first outlined the boundaries of the four rock glaciers, from which their shapes and areal
extents can be extracted. An empirical relationship established by Brenning (2005b) was then applied to calculate the rock
glacier thickness (T) from its areal extent (A_{rg}):

220 $$T = 50A_{rg}^{0.2} \, ,$$ (17)

where the area (A_{rg}) is in km². The width of each glacier was quantified as the width of its minimum envelop rectangle. We
took the mean value of the active layer thickness obtained from borehole measurements in the PERMOS network as the input
parameter h_{al} for each rock glacier. The surface slope (α) was calculated based on the SRTM DEM with a spatial resolution
of 30 m. Table 2 lists the values of the above parameters. The permafrost core thickness (h_{core}) can be obtained by subtracting
225 h_{al} from the total thickness T calculated using Eq. 17.

We assumed the volumetric ice content ($\theta_{i,core}$) of the permafrost core to be between 40% and 100%, considering the
prerequisites of the modified ice–debris mixture flow law (Eq. 3) that the debris fraction ($\theta_{d,core}$) should be less than the
threshold (θ_{dc}) (Sect. 3.2.1). We varied the ice content ($\theta_{i,core}$) by 1% in each step to model the corresponding surface
velocities (u_s). We fixed the air content in the permafrost core as 7.5%, which is a mean value of the air fraction in ice-rich
230 permafrost samples (Arenson and Springman, 2005b). At near 0 °C, the volumetric content of water ($\theta_{w,core}$) displays a
positive correlation with the debris fraction ($\theta_{d,core}$) (Monnier and Kinnard, 2016). Thus, we calculated the $\theta_{d,core}$–$\theta_{w,core}$
correlation based on the data published in Monnier and Kinnard (2015b) and assumed the constitution of the selected rock
glaciers followed the same linear relationship (Fig. 4d). The debris density (ρ_d) was given as 2450 kg/m³ (Monnier and Kinnard,
2016). The density of air (ρ_a) is determined by the elevation of each rock glacier. The ice density (ρ_i) is 916 kg/m³ and the
235 water density (ρ_w) is 1000 kg/m³.

Table 2. Summary of the geometric and structural parameters used in the validation.

Rock glacier	Area (A_{rg}) (km²)	Width (W) (m)	Active layer thickness (h_{al}) (m)	Surface slope (α) (°)
Murtèl-Corvatsch	0.06487	29	3.0	16
Gruben	0.7422	47	2.0	10
Muragl	0.02666	24	4.5	12
Schafberg	0.02715	24	4.8	16

3.2.4 Sensitivity analysis

To explore how uncertainties of the input parameters contribute to the final output of the developed approach, we tested the
response of the model to varying input parameters by performing a series of synthetic sensitivity experiments. For these
240 experiments, we simulated surface velocities of the rock glacier with varying ice fractions and inferred the current ice content

from the velocity constraint. The parameters explored here are detailed in Table 3. A reference scenario is set up with the parameters of Murtèl-Corvatsch rock glacier and labelled as Sc-1.0. We designed eight scenarios extending from Sc-1.0, naming each scenario after a multiplication factor which indicates the ratio between the parameter in each scenario and that in the reference scenario; with the exception of two parameters, namely debris density (ρ_d) and debris fraction in the active layer

245 ($\theta_{d,al}$), where we changed the upper or lower boundary of the value range to be consistent with the usual value range in reality. We performed the sensitivity experiments by varying one parameter at a time while keeping the other variables constant.

Table 3. Parameters of the sensitivity experiments. Scn-1.0 is the reference scenario that adopts the parameters of Murtèl-Corvatsch rock glacier. The other scenarios are designed by multiplying the reference value of each variable with the corresponding factor in their scenario labels.

Scenario	A_{rg} (km^2)	W (m)	α (°)	h_{al} (m)	ρ_d (kg/m^3)	$\theta_{d,al}$ (%)	$\theta_{a,core}$ (%)
Scn-0.2	0.01297	40	3.2	0.6	1450	13	1.5
Scn-0.4	0.02594	80	6.4	1.2	1700	26	3.0
Scn-0.6	0.03892	120	9.6	1.8	1950	39	4.5
Scn-0.8	0.05189	160	12.8	2.4	2200	52	6.0
Scn-1.0	0.06487	200	16	3.0	2450	65	7.5
Scn-1.2	0.07784	240	19.2	3.6	2700	72	9.0
Scn-1.4	0.09081	280	22.4	4.2	2950	79	10.5
Scn-1.6	0.10379	320	25.6	4.8	3200	86	12.0
Scn-1.8	0.11677	360	28.8	5.4	3450	93	13.5

250 **3.2.5 Model application**

We applied the validated model with the optimal parameterisation scheme to infer ice content of the coherently moving part of five rock glaciers in the Khumbu and Lhotse Valleys. The geometric and structural data used as input parameters are detailed in Table 4. Area, width, and slope angle are quantified using the same method as described in Sect. 3.2.3. Active layer thickness was determined as the mean value over the extent of each rock glacier during 2006–2017 from the European Space Agency

255 Permafrost Climate Change Initiative Product (ESA CCI) (Obu et al., 2020). The same empirical relation for calculating rock glacier thickness as used in the validation procedure was adopted here to obtain the thickness parameter. The surface velocity constraint is the range of InSAR-derived downslope velocity during the observed period (Sect. 3.2.2); except for Tobuche RG where the abnormal value in 2015 is removed from the range (see Sect. 4.1 for details). Finally, we calculated the water volume equivalent to estimate the amount of water stored in rock glaciers by considering the inferred ice content, areal extent, and

260 permafrost core thickness.

Table 4. Summary of the geometric and structural parameters used for inferring ice content of the coherently moving part of rock glaciers in the study area.

Rock glacier	Area (A_{rg}) (km^2)	Width (W) (m)	Active layer thickness (h_{al}) (m)	Surface slope (α) (°)
Kala-Patthar	0.074	240	0.68	9
Kongma	0.077	300	0.83	13
Lingten	0.094	240	0.65	20
Nuptse	0.234	400	0.30	13
Tobuche	0.128	400	1.67	16

4 Results

In this section we first summarise the surface kinematic characteristics of rock glaciers in Khumbu and Lhotse Valleys measured by InSAR. Then we show the results of model validation and sensitivity experiments. Finally, we present the inferred ice contents and estimated water storage of rock glaciers in the study area.

4.1 InSAR-derived surface kinematics of rock glaciers

We used InSAR to derive the downslope surface velocities of five rock glaciers situated in the study region. Surface kinematics of debris-covered glaciers were also quantified and presented in Fig. S1 and S2 in the supplementary materials.

Figure 5 shows the time series of the InSAR-derived surface velocities of the rock glacier coherently moving parts. We observe that the median and mean velocities of each landform have similar values, and both are capable of characterising the kinematic status of the landforms. By selecting the mean velocity as the representative value, most rock glaciers, except for Tobuche, moved at a nearly stable rate, ranging from 5 cm yr^{-1} to 30 cm yr^{-1} during the observational period, with the largest standard deviation being 3.4 cm yr^{-1} for Lingten. The maximum velocity represents the local extreme of downslope motion and was as high as 112.1±12.4 cm yr^{-1} for Lingten during 2019/07/15–2019/08/26. Tobuche displayed similar stable behaviour before 2010 but had accelerated by more than four times from 14.9±0.2 cm yr^{-1} to 81.4±2.4 cm yr^{-1} since 2010. The maximum velocity reached was 181.0±57.4 cm yr^{-1} for the period 2015/03/18–2015/03/22. However, the associated uncertainties during this period were high: the relative uncertainties of mean, median, and maximum velocity were 2.9%, 38.2%, and 31.7%, respectively. Therefore, the acceleration of Tobuche cannot be confidently revealed by our data. The extents of coherently moving parts of the five rock glaciers are presented in Fig. 6, with the average velocities derived from the interferograms obtained during the past several years.
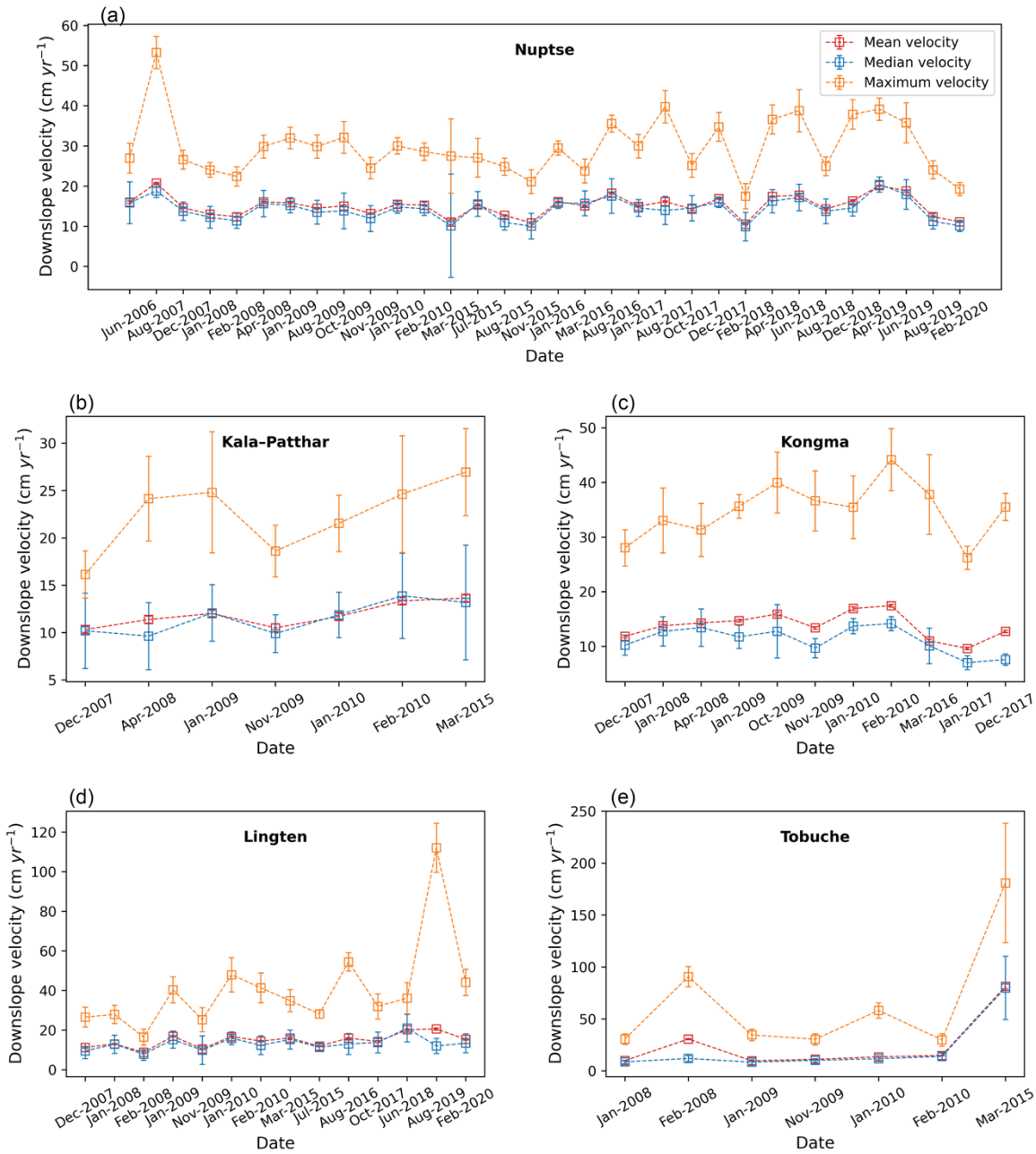
285

Figure 5: Time series of the InSAR-derived downslope velocities of the landforms. The spatial mean velocities and uncertainties during each period are shown (red squares and error bars) as well as the median (blue) and maximum (orange) velocities.
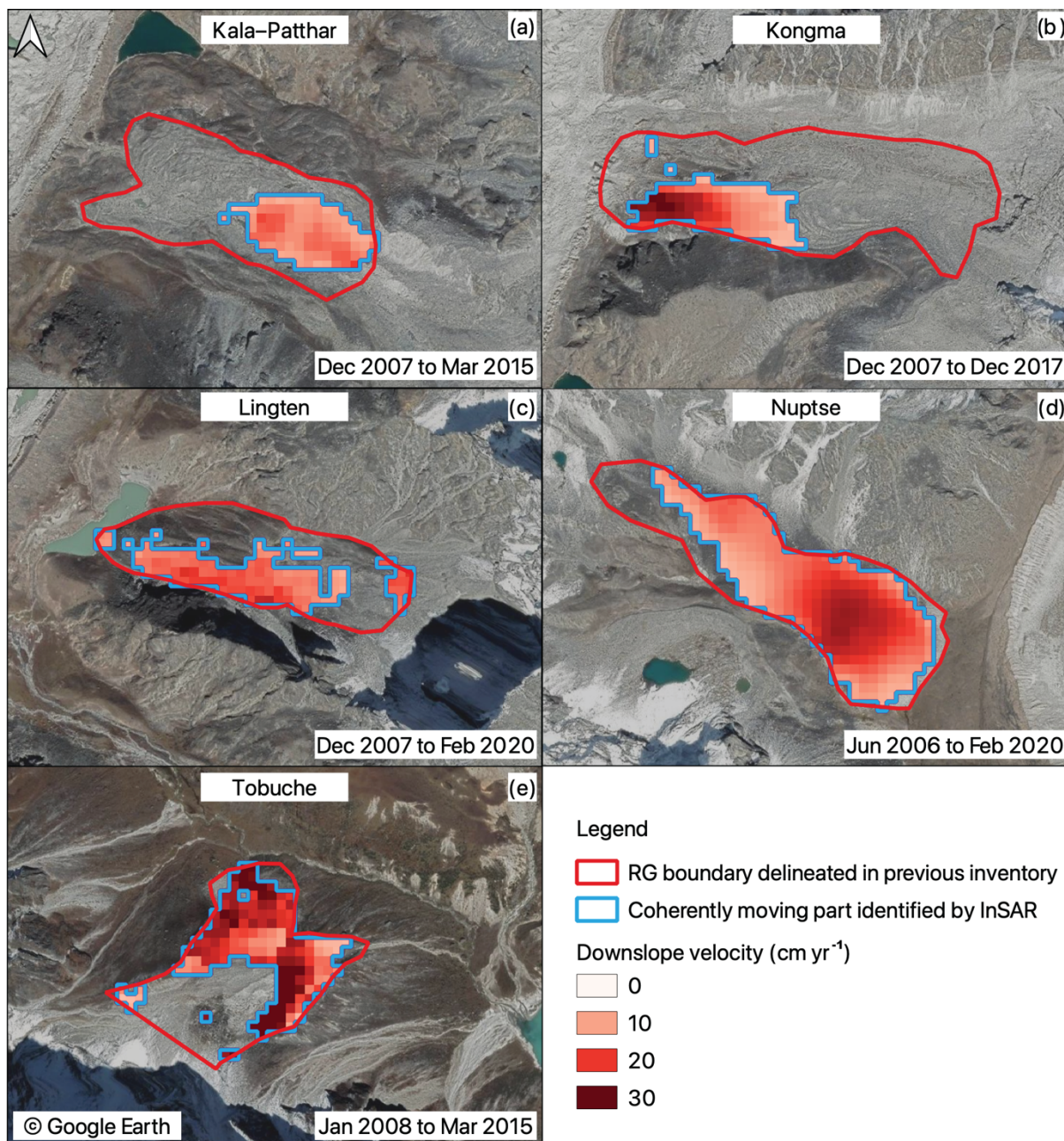
Figure 6: Velocity field maps show the average movement rates of the coherently moving parts of the five rock glaciers (blue outlines) in the study area. The boundaries of the landforms delineated in previous inventorying work are in red polygons. The background are Google Earth images.

4.2 Model validation

With the input parameters and model setup as detailed in Sect. 3.2.3, we simulated the surface velocities (u_s) of each rock glacier using Schemes 1–3. Uncertainties, generated through the statistical analysis used to establish the model (as shown in

295 Fig. 4), have all been considered in the simulation. We used the annual mean surface velocities, calculated from the Terrestrial Ground Survey data (PERMOS, 2019), as the constraint for inferring the ice content.

For each rock glacier, an inferred ice content range is derived based on the velocity constraint and modelled $u_s - \theta_{i,core}$ relationship. The median of the range is selected as the inferred ice content and compared with the reference ice content, which is taken as the average value of the estimated ice content based on previous field measurements (Cicoira et al., 2019a; Arenson

300 et al., 2002; Hoelzle et al., 1998; Barsch et al., 1979).

Comparing the reference and inference ice content from the three schemes, Scheme 2 is the optimal one for the following two reasons: (1) the reference ice content is within the range inferred from Scheme 2 (Fig. 8); (2) Scheme 2 gives the smallest average bias (8.4%) compared with Scheme 1 (12.9%) and Scheme 3 (13.3%) (Table 5). However, the above bias is not statistically useful for correcting the modelling results due to the limited amount of validation data.
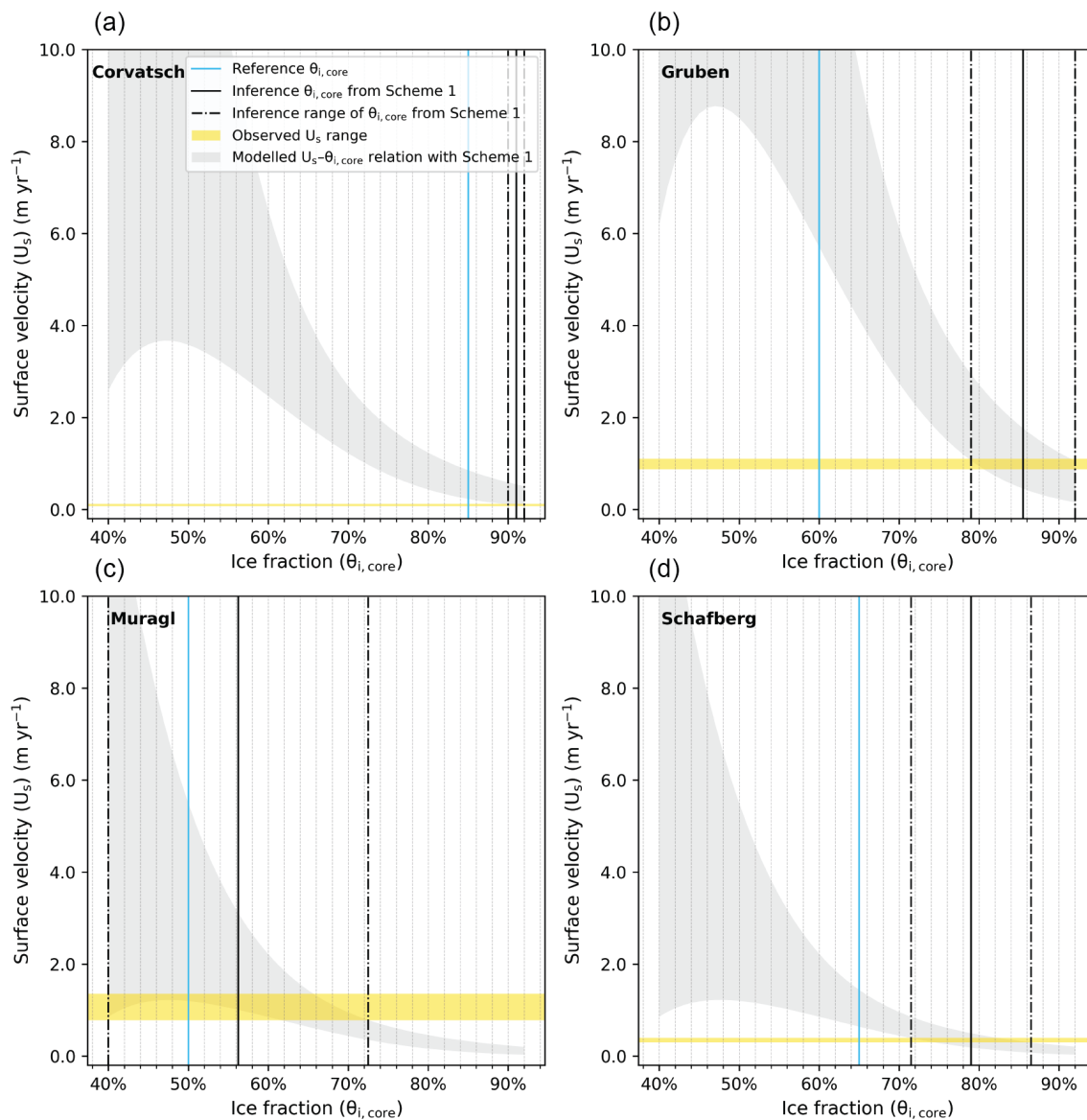
305

Figure 7: Modelled relationships (grey shaded areas) between the ice fraction ($\theta_{i,core}$) and the surface velocity (u_s) of 95% confidence intervals for the four RGs monitored in the PERMOS network with model parameterisation Scheme 1. The ranges of the observed velocities (yellow bands) are used as velocity constraints for inferring ice content from the modelled relationships. Also shown are the reference ice content obtained from previous field-based surveys (blue lines). The inference ice contents are the mean values
310 **(solid black lines) with the estimated ranges (dash-dotted black lines).**
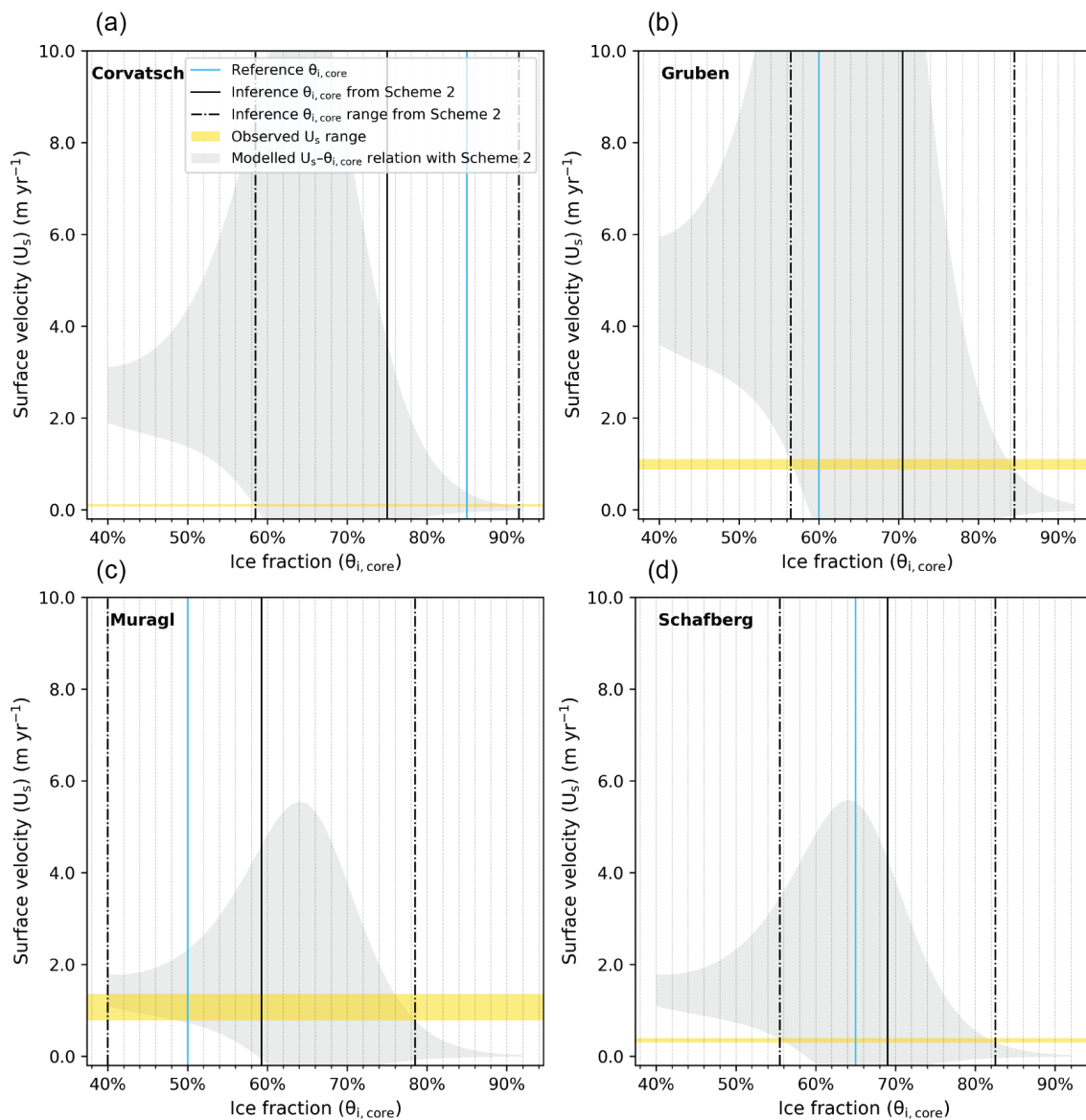
Figure 8: Similar to Fig. 7, but showing results obtained based on model parameterisation Scheme 2.
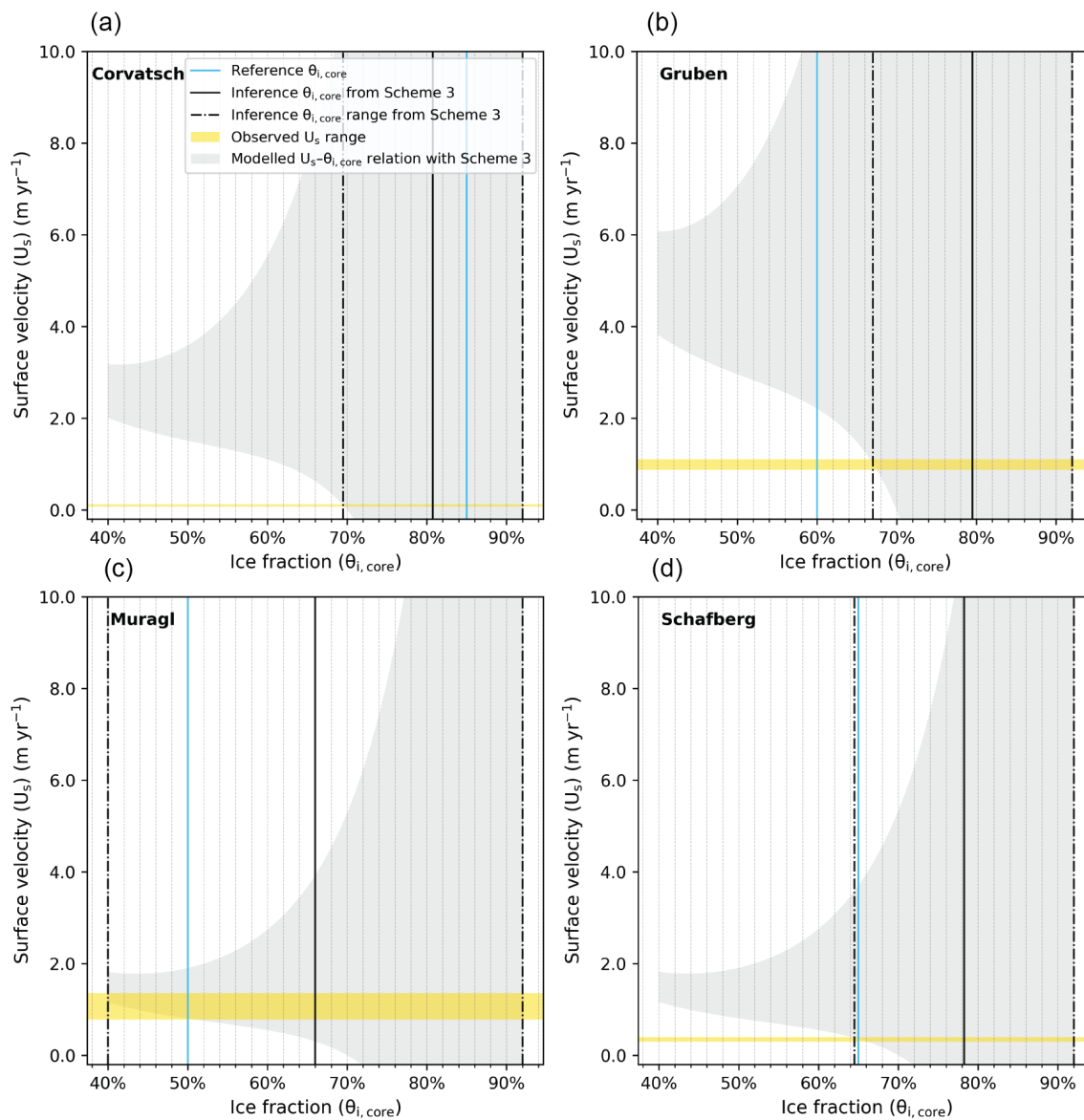
Figure 9: Similar to Fig. 7 and 8, but showing results derived from model parameterisation Scheme 3.

315

320 **Table 5. Summary of the reference and inference ice contents derived from the three model parameterisation schemes. The values in brackets following the inference ice contents give the corresponding bias from the reference ice contents.**

Rock glacier	**Reference** (%)	Inference and bias		
		Scheme 1(%)	Scheme 2 (%)	Scheme 3 (%)
Murtèl-Corvatsch	85	91 (7)	75 (–10)	81 (–4)
Gruben	60	85 (25)	71 (11)	80 (20)
Muragl	50	56 (6)	59 (9)	66 (16)
Schafberg	65	79 (14)	69 (4)	78 (13)
Mean bias	–	12.9	8.4	13.3

4.3 Model sensitivity

The results of sensitivity experiments are shown, normalised to the corresponding values of the reference scenario (Scn-1.0),
in Fig. 10. We observe that the inference result remains stable in response to most varying parameters, with a bias of less than
325 5%, relative to the reference scenario (Scn-1.0). Surface slope angle influences the result most: in the extreme scenario (Scn-
0.2), the inferred ice content can be altered by 15%. In non-extreme cases (e.g., Scn-0.8, Scn-0.6), the influences of varying
slope angles can be well constrained within the 5% range. In general, the model is insensitive to the uncertainties of any single
input parameter.
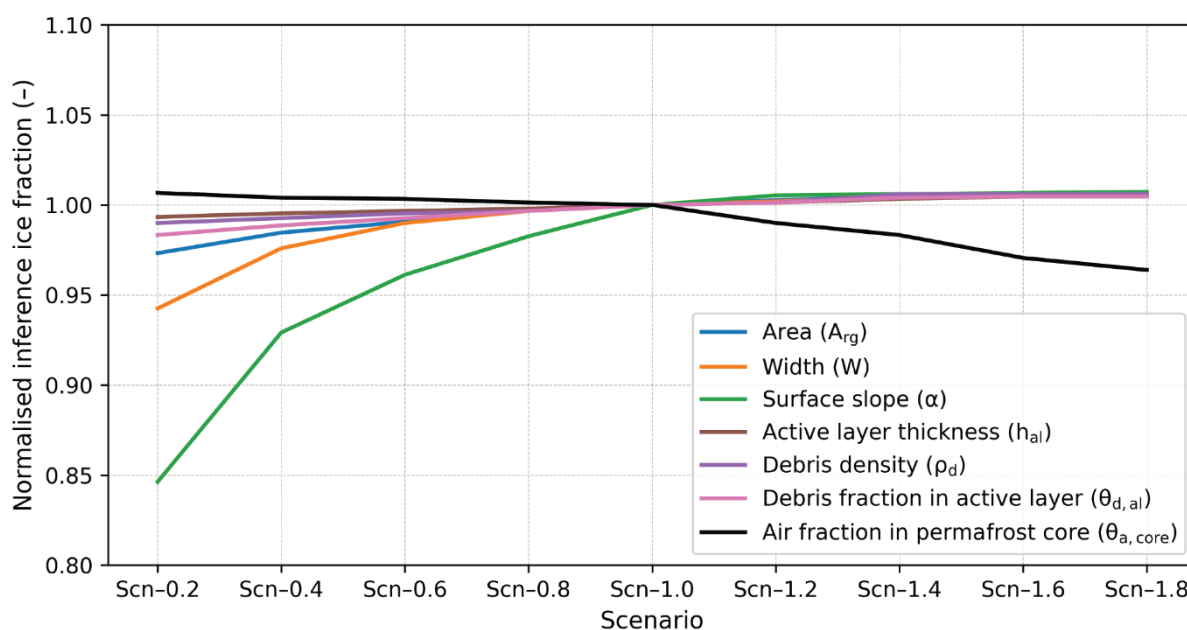
330 **Figure 10: Normalised inference ice fractions from sensitivity experiments with different parameter scenarios. The varying parameters include rock glacier area (blue line), width (orange line), surface slope (green line), active layer thickness (brown line), debris density (purple line), debris fraction in the active layer (pink line), and air faction in permafrost core (black line).**

4.4 Modelled ice contents

Figure 11 and Table 6 present the inference ice contents of rock glaciers in the study area. The inferred average ice fractions
335   of the landforms are in the range of 71.0–75.3%; the water volume equivalent ranges from 1.40 to 5.92 million m³ for individual
landforms. The maximum range of ice fraction is estimated to be 57.5–92.0%; the corresponding water volume equivalent
ranges from 1.13 to 7.24 million m³. Nuptse stores the most ice by volume due to its largest dimensions. The total amount of
water stored in each of the five rock glaciers lies between 10.61 and 16.54 million m³, with an average value of 13.57 million
m³.
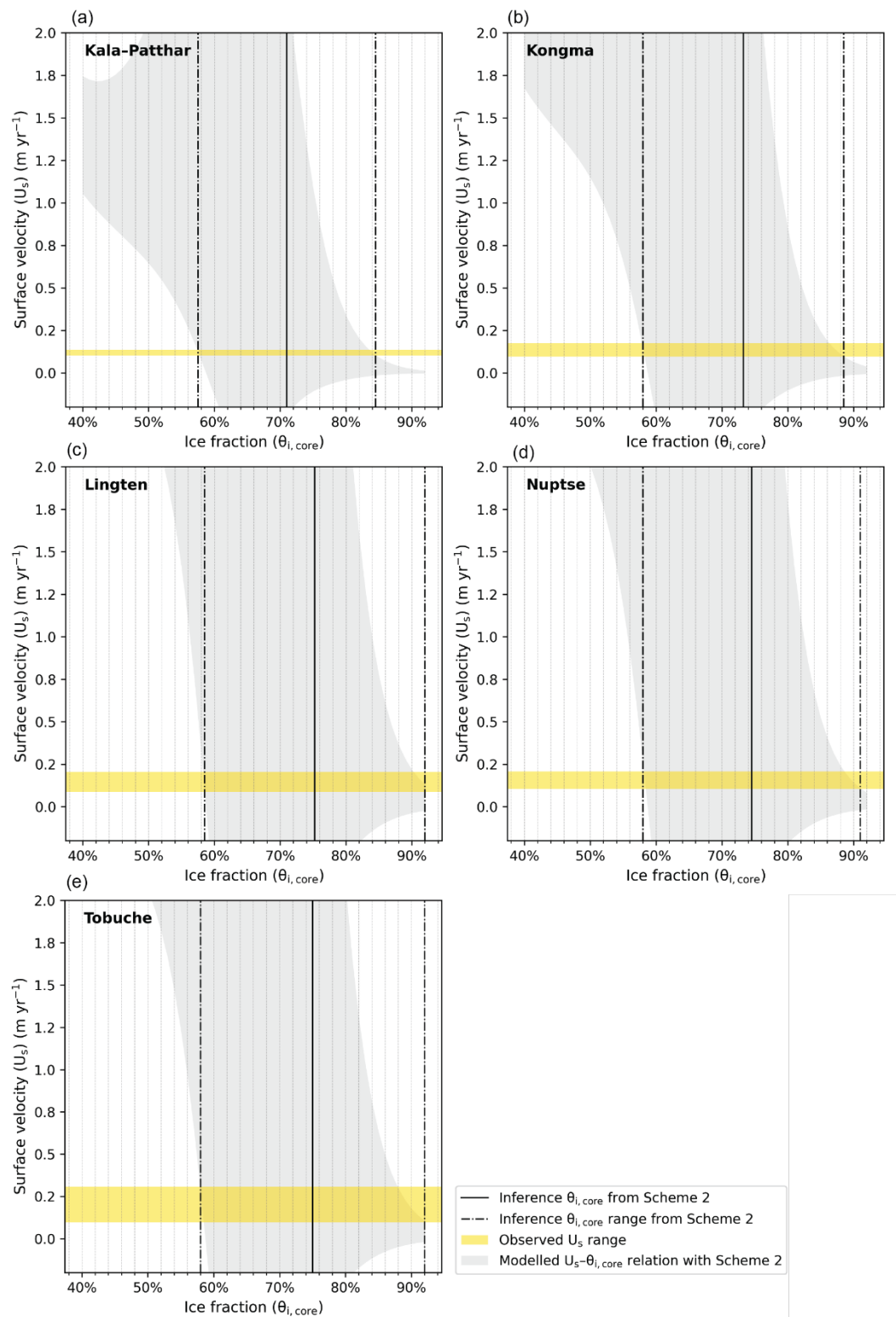
Figure 11: Modelled relationships between the ice fraction ($\theta_{i,core}$) and the surface velocity (u_s) of 95% confidence intervals for the five RGs in Khumbu Valley with model parameterisation Scheme 2 (grey shaded areas). The ranges of the InSAR-derived velocities are shown (yellow bands), which are used as the velocity constraints for inferring ice contents from the modelled relationships. The upper and lower boundaries of the estimated ice contents are within the range outlined by the dash-dotted black lines and the solid black lines show the mean values representing the inference ice contents.

Table 6. Modelled average ice contents, as well as the minimum and maximum estimates (in brackets) of rock glaciers in Khumbu and Lhotse Valleys and the corresponding water volume equivalents.

Rock glacier	Inference ice content (%)	Water volume equivalent (million m³)
Kala-Patthar	71.0 (57.5–84.5)	1.40 (1.13–1.66)
Kongma	73.3 (58.0–88.5)	1.50 (1.19–1.82)
Nuptse	74.5 (58.0–91.0)	5.92 (4.61–7.24)
Lingten	75.3 (58.5–92.0)	1.98 (1.54–2.42)
Tobuche	75.0 (58.0–92.0)	2.77 (2.14–3.40)

5 Discussion

The following subsections firstly investigate the potential water storage of rock glaciers over the Nepalese Himalaya by extrapolating the estimated water storage in the Khumbu and Lhotse Valleys (Sect. 5.1). We then discuss the validity of the approach developed in this study for inferring ice content by analysing the general assumptions and design of the surface-velocity-constrained model (Sect. 5.2), based upon which we discuss the application of the method to large-scale regions and further improvements (Sect. 5.3).

5.1 Potential water storage in rock glaciers in the Nepalese Himalaya

The inferred average ice content of the five rock glaciers in the study area lies within a narrow range (71.0–75.3%), mainly due to their similar observed downslope velocities (5–30 cm yr⁻¹), used as modelling constraints (Fig. 5; Fig. 6; Sect. 4.1). In general, rock glaciers typically creep at a rate ranging from decimetre to several meters per year (Delaloye and Echelard, 2020), thus the average ice content of the five rock glaciers may not be able to represent the motion of all rock glaciers situated in the entire mountain range.

A previous study has compiled an inventory including 4226 intact rock glaciers over the Nepalese Himalaya, and a first-order estimate has indicated that these landforms contain between 16.72 and 25.08 billion m³ of water (Jones et al., 2018b). By extrapolating from the estimated water storage in the five rock glaciers found in this study, the total amount of water stored in all the intact rock glaciers ranges from 8.97 to 13.98 billion m³ over the entire Nepalese Himalaya, which is in the same magnitude predicted by the previous research (Jones et al., 2018b). In the Nepalese Himalaya, the ratio between the amount of water stored in rock glaciers (11.47 billion m³) and in glaciers (197.63 billion m³) is 1:17. By using the minimum and maximum inference values, the estimated ratio ranges between 1:21 and 1:13. Our modelling-based results are lower than

earlier estimates (1:9), yet reveal higher hydrological importance than across the Himalayas (1:24) (Jones et al., 2018b; Jones et al., 2021).

5.2 Validity of general assumptions and model design

370   Our aim was to develop a rheological model that allows for inferring ice content of rock glaciers in areas where in situ investigations are scarce. To achieve this objective, certain simplifications have been applied to the model setup. Here we discuss the validity of the method through the following six aspects of the model assumptions and design, including (1) assumption of a steady-state rock glacier creep, (2) homogeneous warm permafrost hypothesis, (3) neglect of shear horizon in the model design, (4) accuracy of rock glacier thickness derivation, (5) identification of the coherently moving part of rock

375   glaciers, and (6) generalisation of statistical relationships derived from Las Liebres rock glacier.

5.2.1 Steady-state creep of rock glaciers

By using the adapted form of Glen's flow law (Eq. 2), we primarily assume the rock glacier movement to be steady-state creep driven by viscoelastic deformation of the ice–debris mixture (Moore, 2014). This premise indicates that our method is applicable to rock glaciers currently moving at a relatively stable rate. Recent research has reported abrupt and significant

380   acceleration of rock glaciers triggered by abnormal surface warming events (Delaloye et al., 2013). These destabilised rock glaciers are beyond the applicability of our method. In this study, we quantified surface kinematics of rock glaciers over multiple years to quantify the stability of the rock glacier motion. The seasonal variations in creep rate are neglected and sudden acceleration events are excluded in the velocity range used as the model constraint (Sect. 4.1).

We also exclude the component of basal sliding processes in our model design (Fig. 3), which operates at the base of some

385   rock glaciers, as observed in the Tien Shan (Harrison unpubl.). This is not surprising; many clean glaciers undergo basal sliding in certain situations (e.g., Vivian and Bocquet, 1973) although, a debris-rich layer with high water content at the base undergoes enhanced deformation and some sliding (e.g., Boulton and Jones, 1979; Echelmeyer and Wang, 1987). This process also occurs in rock glaciers with a high ice content and is accompanied by the disruption of sediment and vegetation at the front of such features. The kinematics of these rock glaciers cannot be appropriately simulated by our current approach.

390   ### 5.2.2 Homogeneous warm permafrost

Ground temperature is one of the factors controlling the creep parameter (A) (Eq. 1), as described by the Arrhenius relation (Mellor and Testa, 1969). As ground temperature changes with depth, primarily due to heat diffusion, creep parameter (A) varies along the vertical profile of the rock glacier. Previous studies implemented different relationships between creep parameter and temperature, and integrated a heat diffusion model (proposed by Carslaw and Jaeger, 1959) to consider this

395   effect (Azizi and Whalley, 1996; Arenson and Springman, 2005a; Kääb et al., 2007; Ladanyi, 2003).

In our model design, we use the effective viscosity (B) to absorb the intricate effects of strain enhancement factor (E), threshold stress (τ_{th}), and most importantly, the creep parameter (A) (Eq. 3), which reduces the number of input parameters and allows

for developing an empirical relationship between effective viscosity and ice content based on an existing observational dataset and laboratory findings (Eq. 13). The data and relationship between variables we used for model calibration are derived from

400   observations of rock glaciers situated in a warm permafrost environment (>–3°C) (Monnier and Kinnard, 2016; Arenson and Springman, 2005a)

Measurements of ground temperature in the study area are scarce in general. However, we infer that these rock glaciers develop in a warm permafrost environment for the following reasons: (1) the landforms are located near or below the altitudinal limit of permafrost distribution in Nepal (Sect. 2) (Fujii and Higuchi, 1976; Jakob, 1992), indicating that the local environment is

405   at the critical condition of permafrost occurrence; (2) based on empirical relationships between mean annual ground temperature (MAGT), mean annual air temperature, latitude, and altitude, the estimated MAGT is >0.5°C, which suggests that permafrost in this area is in a warm and unstable condition (Nan et al., 2002; Zhao and Sheng, 2015).

5.2.3 Neglect of shear horizon

The shear horizon is discovered from borehole investigations and is defined as the thin layer situated at more than ten meters

410   deep where the majority of internal deformation takes place (Arenson et al., 2002; Buchli et al., 2018; Haeberli et al., 1998). Field observations and numerical modelling suggest that unfrozen water within the shear horizon plays an important role in controlling the seasonal variations in rock glacier creep (Buchli et al., 2018; Cicoira et al., 2019b; Kenner et al., 2019). This short-term feature of rock glacier kinematics is insignificant to modelling the relationship between ice content and multi-annual average movement velocity in our study.

415   Previous studies have considered the enhanced deformation occurring in the shear horizon additionally, but it requires detailed knowledge of the internal structure, i.e., the depth of shear horizon (Frehner et al., 2015; Ladanyi, 2003). To tackle the issue of data insufficiency of internal rock glacier structure in this study area – as with most permafrost areas – we neglect the distinct rheology in the shear horizon and assume a constant effective viscosity instead. This simplification has also been adopted in other research aiming at studying rock glacier dynamics over a large-scale extent (Cicoira et al., 2020).

420   ### 5.2.4 Accuracy of rock glacier thickness derivation

The accuracy of rock glacier thickness is discussed here because it influences the surface kinematics most significantly. As shown in Eq. 8, the surface velocity is proportional to the thickness to the power of $n + 1$, resulting from the vertical integration of Eq. 7. We adopt the empirical relationship between rock glacier area and thickness (Eq. 17) based on field observations in the Andes (Brenning, 2005a). The derived thicknesses of the four rock glaciers in the Swiss Alps, used for validation, are

425   consistent with previous in situ measurements. However, another rock glacier, namely Ritigraben, situated in the same region, does not follow this empirical relationship and has a bias as large as ten meters compared with the field estimates. We also test a linear relationship between surface slope angle and thickness, recently established by Cicoira et al. (2020). The accuracies of the results turn out to be at the same level, with four out of five rock glaciers having good estimation results (Table 7). Thus,

the uncertainty introduced by thickness derivation when applied to rock glaciers without known information of structure is
430   unavoidable.

Table 7. Estimated rock glacier thickness derived from the thickness–area relationship used in this study (T_{area}) (Eq. 17), and the corresponding bias relative to in situ measured thickness (Barsch et al., 1979; Cicoira et al., 2019a; Arenson et al., 2002; Hoelzle et al., 1998). The rock glacier thickness derived from slope angle (T_{slp}) proposed by Cicoira et al. (2020), and the associated bias.

Rock glacier	T_{area} and bias (m)	T_{slp} and bias (m)	T_{ref} (m)
Murtèl-Corvatsch	29 (2)	26.2 (–0.8)	27
Gruben	47 (–3)	28 (–22)	50
Muragl	24 (4)	19 (–1)	20
Schafberg	24 (–1)	20.8 (–4.2)	25
Ritigraben	28 (10)	12.7 (–5.3)	18

5.2.5 Identification of the coherently moving part of rock glaciers

435   Taking advantage of the multi-temporal observations and continuous spatial coverage of the InSAR measurements, we define
the coherently moving part of each rock glacier in our study area (Fig. 6; Sect. 3.1) and infer the ice content of the coherently
moving part using the developed modelling approach. We introduce this concept because it corresponds with the general model
setup (Fig. 3). Moreover, with the assistance of displacement maps generated by InSAR, the defined boundary of coherently
moving rock glacier avoids the ambiguities involved when delineating rock glaciers solely based on geomorphologic features
440   from a highly dynamic environment where complex glacial, periglacial, and paraglacial processes take place (Jones et al.,
2019; Delaloye and Echelard, 2020). In addition, defining the coherently moving part associates with the uncertainty in the
rock glacier area, which is unlikely to affect the modelling result significantly due to the insensitive response of our model to
this input parameter (Fig. 10). Finally, employing this kinematics-based definition, may also contribute to the currently
inevitable uncertainties in thickness estimation (Sect. 5.2.4), as Eq. 17 (proposed by Brenning, 2005b) uses rock glacier area
445   as a variable, without considering the landform activity.

5.2.6 Generalisation of statistical relationships derived from Las Liebres rock glacier

The model developed in this study essentially relies on statistical relationships, especially the effective viscosity–ice content
relationship, derived from geophysical surveys conducted on Las Liebres rock glacier in the Andes (Monnier and Kinnard,
2015b). Applying the calibrated model to rock glaciers in other areas is primarily based on the assumption that a common flow
450   law governs the rheology of rock glaciers developed in warm permafrost environment, irrespective of locality. In addition to
the general hypothesis, we tackled this issue in two ways. First, we validated the model using samples from a different region,
i.e., the Swiss Alps (Sect. 3.2.3). Secondly, the uncertainties introduced by the statistical analysis have all been quantified in
the validation and inference procedures, which leads to a wide range of the inference ice contents (Sect. 3.2.3 and 4.4).

5.3 Application of the model and outlook

455 By adopting the assumptions and setup as discussed in Sect. 5.2, we firstly present an approach for estimating ice content of rock glaciers with simple input parameters, including the planar shape (area and width), surface slope angle, active layer thickness, and surface velocity, all of which can be obtained directly or derived from remote sensing techniques and products. Therefore, this established method for estimating the amount of ice stored in numerous rock glaciers with well-quantified uncertainties is ready to be applied to many remote alpine environments.

460 To improve the performance of the approach, more data obtained from field and geophysical investigations, especially detailed data of rock glacier composition, can be integrated in the future to calibrate and validate the empirical rheological model. More reliable methods for estimating rock glacier thickness will also improve the accuracy of the modelling results.

6 Conclusions

We develop an empirical rheological model for inferring ice content of rock glaciers and apply it to estimate the water storage
465 of rock glaciers situated in the Khumbu and Lhotse Valleys using surface-velocity-constraints derived from InSAR measurements. The main findings are summarised as follows:

(1) An empirical rheological model is presented in this study for estimating ice content of rock glaciers using five input parameters, namely rock glacier area, width, surface slope angle, active layer thickness, and surface velocity, all of which can be obtained from readily available remote sensing products or emerging datasets.

470 (2) Mean downslope velocities of the rock glaciers situated in Khumbu and Lhotse Valleys ranged from 5 cm yr^{-1} to 30 cm yr^{-1} and mostly remained stable during the observational period (2006–2020).

(3) The inferred average ice contents of rock glaciers in Khumbu and Lhotse Valleys are in the range of 71.0–75.3%; the water volume equivalent ranges from 1.40 to 5.92 million m^3 for individual landforms. Nuptse RG stores the most ice due to its largest dimensions among the five studied rock glaciers.

475 (4) The inference range of ice content of the landforms lies between 57.5 and 92.0%. Total amount of water stored in the five rock glaciers in Khumbu and Lhotse Valleys ranges from 10.61 to 16.54 million m^3, with an average value of 13.57 million m^3.

(5) Considering previous estimates and extrapolating from our inference results in Khumbu and Lhotse Valleys, the total amount of water stored in rock glaciers over the Nepalese Himalaya is in the magnitude of 10 billion m^3, and the ratio between
480 water storage in rock glaciers and glaciers ranges from 1:13 to 1:21, averaging at 1:17.

This study demonstrates the effectiveness of inferring ice content of rock glaciers by using a surface-velocity-constrained model. The estimated ice content and water storage in the study area highlights the hydrological significance of rock glaciers in the Nepalese Himalaya. The approach developed here can be readily applied to other alpine permafrost regions where rock glaciers are widespread for a preliminary water resource evaluation.
Code and data availability

The source code of ISCE is available at https://github.com/isce-framework/isce2. The ALOS PALSAR and ALOS-2 PALSAR-2 data are copyrighted and provided by the Japan Aerospace Exploration Agency through the EO-RA2 project ER2A2N081. Data for the rock glacier kinematics in the Swiss Alps are available at http://www.permos.ch/data.html. The ESA CCI permafrost data are available at http://catalogue.ceda.ac.uk/uuid/1f88068e86304b0fbd34456115b6606f. The code of the modelling approach for estimating ice content will be provided by Yan Hu upon request.

Author contribution

YH developed the code, performed the data analysis and interpretation, visualised the results, and wrote the majority of the manuscript. SH conceptualised the research goal, supervised the study, and wrote Sect. 1 of the draft. LL advised YH and actively helped the investigation process. JLW helped formulate the initial framework of the method and collect research data. All the authors contributed to the reviewing and editing of the manuscript.

Competing interests

The authors declare that they have no conflict of interest.

Acknowledgements

We thank Juliet Ermer for helping to digitalize landform boundaries used in this work.

Financial support

This work is supported by CUHK Global Scholarship Programme, CUHK-Exeter Joint Centre for Environmental Sustainability and Resilience (ENSURE, 4930821), the Hong Kong Research Grants Council (CUHK14303417 and HKPFS PF16-03859), and CUHK Direct Grant for Research (405348).

References

Arenson, L., Hoelzle, M., and Springman, S.: Borehole deformation measurements and internal structure of some rock glaciers in Switzerland, Permafrost Periglac., 13, 117-135, https://doi.org/10.1002/ppp.414, 2002.

Arenson, L., and Springman, S.: Mathematical descriptions for the behaviour of ice-rich frozen soils at temperatures close to 0 C, Can. Geotech. J., 42, 431-442, https://doi.org/10.1139/t04-109, 2005a.

Arenson, L., and Springman, S.: Triaxial constant stress and constant strain rate tests on ice-rich permafrost samples, Can. Geotech. J., 42, 412-430, https://doi.org/10.1139/t04-111, 2005b.

Azizi, F., and Whalley, W. B.: Numerical modelling of the creep behaviour of ice-debris mixtures under variable thermal regimes, in: International Offshore and Polar Engineering Conference Proceedings, The Sixth International Offshore and Polar Engineering Conference, Los Angeles, 1996, WOS:A1996BF95F00053, 362-366,

Azócar, G. F., and Brenning, A.: Hydrological and geomorphological significance of rock glaciers in the dry Andes, Chile (27°-33°S), Permafrost Periglac., 21, 42-53, https://doi.org/10.1002/ppp.669, 2010.

Barsch, D., Fierz, H., and Haeberli, W.: Shallow core drilling and borehole measurements in the permafrost of an active rock glacier near the Grubengletscher, Wallis, Swiss Alps, Arctic Alpine Res., 11, 215-228, https://doi.org/10.2307/1550646, 1979.

Berthling, I., Etzelmüller, B., Isaksen, K., and Sollid, J. L.: Rock glaciers on Prins Karls Forland. II: GPR soundings and the development of internal structures, Permafrost Periglac., 11, 357-369, https://doi.org/10.1002/1099-1530, 2000.

Berthling, I.: Beyond confusion: Rock glaciers as cryo-conditioned landforms, Geomorphology, 131, 98-106, https://doi.org/10.1016/j.geomorph.2011.05.002, 2011.

Boulton, G. S., and Jones, A. S.: Stability of temperate ice caps and ice sheets resting on beds of deformable sediment, J. Glaciol., 24, 29-43, https://doi.org/10.3189/S0022143000014623, 1979.

Brenning, A.: Geomorphological, hydrological and climatic significance of rock glaciers in the Andes of Central Chile (33-35 degrees S), Permafrost Periglac., 16, 231-240, https://doi.org/10.1002/ppp.528, 2005a.

Brenning, A.: Climatic and geomorphological controls of rock glaciers in the Andes of Central Chile, Humboldt-Universität zu Berlin, Mathematisch-Naturwissenschaftliche Fakultät II, 2005b.

Buchli, T., Kos, A., Limpach, P., Merz, K., Zhou, X. H., and Springman, S. M.: Kinematic investigations on the Furggwanghorn Rock Glacier, Switzerland, Permafrost Periglac., 29, 3-20, https://doi.org/10.1002/ppp.1968, 2018.

Carslaw, H. S., and Jaeger, J. C.: Conduction of heat in solids, Oxford Science Publications. Clarendon Press, Oxford, 1959.

Chen, C. W., and Zebker, H. A.: Phase unwrapping for large SAR interferograms: statistical segmentation and generalized network models, IEEE T. Geosci Remote., 40, 1709-1719, https://doi.org/10.1109/TGRS.2002.802453, 2002.

Cicoira, A., Beutel, J., Faillettaz, J., Gartner-Roer, I., and Vieli, A.: Resolving the influence of temperature forcing through heat conduction on rock glacier dynamics: a numerical modelling approach, The Cryosphere, 13, 927-942, https://doi.org/10.5194/tc-13-927-2019, 2019a.

535   Cicoira, A., Beutel, J., Faillettaz, J., and Vieli, A.: Water controls the seasonal rhythm of rock glacier flow, Earth Planet Sc. Lett., 528, https://doi.org/10.1016/j.epsl.2019.115844, 2019b.

Cicoira, A., Marcer, M., Gärtner-Roer, I., Bodin, X., Arenson, L. U., and Vieli, A.: A general theory of rock glacier creep based on in-situ and remote sensing observations, Permafrost Periglac., https://doi.org/10.1002/ppp.2090, 2020.

Corte, A.: The Hydrological Significance of Rock Glaciers, J. Glaciol., 17, 157-158, https://doi.org/10.3189/s0022143000030859, 1976.

540   Croce, F. A., and Milana, J. P.: Internal structure and behaviour of a rock glacier in the Arid Andes of Argentina, Permafrost Periglac., 13, 289-299, https://doi.org/10.1002/ppp.431, 2002.

Cuffey, K., and Paterson, W. S. B.: The physics of glaciers, 4th ed., Butterworth-Heinemann/Elsevier, Burlington, MA, 2010.

Delaloye, R., Morard, S., Barboux, C., Abbet, D., Gruber, V., Riedo, M., and Gachet, S.: Rapidly moving rock glaciers in Mattertal, Geogr. Helv., 21-31, 2013.

545   Delaloye, R., and Echelard, T.: Towards standard guidelines for inventorying rock glaciers: Baseline concepts version 4.0, https://bigweb.unifr.ch/Science/Geosciences/Geomorphology/Pub/Website/IPA/Guidelines/V4/200117_Baseline_Concepts_Inventorying_ Rock_Glaciers_V4.pdf, 2020.

Echelmeyer, K., and Wang, Z.: Direct Observation of Basal Sliding and Deformation of Basal Drift at Sub-Freezing Temperatures, J. Glaciol., 33, 83-98, https://doi.org/10.3189/S0022143000005396, 1987.

550   Florentine, C., Skidmore, M., Speece, M., Link, C., and Shaw, C. A.: Geophysical analysis of transverse ridges and internal structure at Lone Peak Rock Glacier, Big Sky, Montana, USA, J. Glaciol., 60, 453-462, https://doi.org/10.3189/2014jog13j160, 2014.

Frehner, M., Ling, A. H. M., and Gärtner-Roer, I.: Furrow-and-ridge morphology on rockglaciers explained by gravity-driven buckle folding: A case study from the Murtèl rockglacier (Switzerland), Permafrost Periglac., 26, 57-66, https://doi.org/10.1002/ppp.1831, 2015.

Fujii, Y., and Higuchi, K.: Ground Temperature and its Relation to Permafrost Occurrences in the Khumbu Region and Hidden Valley, 555   Journal of Japanese Society of Snow and Ice., 38, 125-128, https://doi.org/10.5331/seppyo.38.Special_125, 1976.

Fukui, K., Sone, T., Strelin, J. A., Torielli, C. A., and Mori, J.: Ground penetrating radar sounding on an active rock glacier on James Ross Island, Antarctic Peninsula region, Pol Polar Res., 13-22, 2007.

Fukui, K., Sone, T., Strelin, J. A., Torielli, C. A., Mori, J., and Fujii, Y.: Dynamics and GPR stratigraphy of a polar rock glacier on James Ross Island, Antarctic Peninsula, J. Glaciol., 54, 445-451, https://doi.org/10.3189/002214308785836940, 2008.

560   Glen, J. W.: The creep of polycrystalline ice, Proceedings of the Royal Society of London. Series A, Mathematical and Physical Sciences (1934-1990), 228, 519-538, https://doi.org/10.1098/rspa.1955.0066, 1955.

Guglielmin, M., Camusso, M., Polesello, S., and Valsecchi, S.: An old relict glacier body preserved in permafrost environment: The Foscagno rock glacier ice core (Upper Valtellina, Italian central Alps), Arctic AntArctic Alpine Res., 36, 108-116, https://doi.org/10.1657/1523-0430, 2004.

565 Guglielmin, M., Ponti, S., and Forte, E.: The origins of Antarctic rock glaciers: periglacial or glacial features?, Earth Surf Proc Land., 43, 1390-1402, https://doi.org/10.1002/esp.4320, 2018.

Haeberli, W., Hoelzle, M., Kaab, A., Keller, F., Vonder Mühll, D., and Wagner, S.: Ten years after drilling through the permafrost of the active rock glacier Murtél, Eastern Swiss Alps: answered questions and new perspectives, Seventh International Conference on Permafrost, Yellowknife, 1998, 403-410,

570 Haeberli, W., Kaab, A., Wagner, S., Vonder Mühll, D., Geissler, P., Haas, J. N., Glatzel-Mattheier, H., and Wagenbach, D.: Pollen analysis and C-14 age of moss remains in a permafrost core recovered from the active rock glacier Murtel-Corvatsch, Swiss Alps: Geomorphological and glaciological implications, J. Glaciol., 45, 1-8, https://doi.org/10.3189/s0022143000002975, 1999.

Haeberli, W.: Modern research perspectives relating to permafrost creep and rock glaciers: A discussion, Permafrost Periglac., 11, 290-293, https://doi.org/10.1002/1099-1530(200012)11:4, 2000.

575 Hanssen, R. F.: Radar interferometry : data interpretation and error analysis, edited by: NetLibrary, I., Kluwer Academic, Dordrecht Boston, 2001.

Hauck, C.: New concepts in geophysical surveying and data interpretation for permafrost terrain, Permafrost Periglac., 24, 131-137, https://doi.org/10.1002/ppp.1774, 2013.

Hausmann, H., Krainer, K., Bruckl, E., and Mostler, W.: Internal structure and ice content of reichenkar rock glacier (Stubai alps, Austria)
580 assessed by geophysical investigations, Permafrost Periglac., 18, 351-367, https://doi.org/10.1002/ppp.601, 2007.

Hoelzle, M., Wagner, S., Kääb, A., and Vonder Mühll, D.: Surface movement and internal deformation of ice-rock mixtures within rock glaciers in the Upper Engadin, Switzerland, Proceedings of the 7th International Conference on Permafrost, 465-471, 1998.

Hu, Y., Liu, L., Wang, X., Zhao, L., Wu, T., Cai, J., Zhu, X., and Hao, J.: Quantification of permafrost creep provides kinematic evidence for classifying a puzzling periglacial landform, Earth Surf Proc Land., 46, 465-477, https://doi.org/10.1002/esp.5039, 2021.

585 Jakob, M.: Active rock glaciers and the lower limit of discontinuous alpine permafrost, Khumbu-Himalaya, Nepal, Permafrost Periglac., 3, 253-256, 1992.

Jones, D. B., Harrison, S., Anderson, K., and Betts, R. A.: Mountain rock glaciers contain globally significant water stores, Sci Rep., 8, https://doi.org/10.1038/s41598-018-21244-w, 2018a.

Jones, D. B., Harrison, S., Anderson, K., Selley, H. L., Wood, J. L., and Betts, R. A.: The distribution and hydrological significance of rock
590 glaciers in the Nepalese Himalaya, Global Planet Change., 160, 123-142, https://doi.org/10.1016/j.gloplacha.2017.11.005, 2018b.

Jones, D. B., Harrison, S., and Anderson, K.: Mountain glacier-to-rock glacier transition, Global Planet Change., 181, https://doi.org/10.1016/j.gloplacha.2019.102999, 2019.

Jones, D. B., Harrison, S., Anderson, K., Shannon, S., and Betts, R. A.: Rock glaciers represent hidden water stores in the Himalaya, Sci. Total Environ., 145368, https://doi.org/10.1016/j.scitotenv.2021.145368, 2021.

595 Kääb, A., Frauenfelder, R., and Roer, I.: On the response of rockglacier creep to surface temperature increase, Global Planet Change., 56, 172-187, https://doi.org/10.1016/j.gloplacha.2006.07.005, 2007.

Kenner, R., Pruessner, L., Beutel, J., Limpach, P., and Phillips, M.: How rock glacier hydrology, deformation velocities and ground temperatures interact: Examples from the Swiss Alps, Permafrost Periglac., 31, 3-14, https://doi.org/10.1002/ppp.2023, 2019.

Kneisel, C., Hauck, C., Fortier, R., and Moorman, B.: Advances in geophysical methods for permafrost investigations, Permafrost Periglac.,
600 19, 157-178, https://doi.org/10.1002/ppp.616, 2008.

Knight, J., Harrison, S., and Jones, D. B.: Rock glaciers and the geomorphological evolution of deglacierizing mountains, Geomorphology, 324, 14-24, https://doi.org/10.1016/j.geomorph.2018.09.020, 2019.

Krainer, K., Bressan, D., Dietre, B., Haas, J. N., Hajdas, I., Lang, K., Mair, V., Nickus, U., Reidl, D., Thies, H., and Tonidandel, D.: A 10,300-year-old permafrost core from the active rock glacier Lazaun, southern Ötztal Alps (South Tyrol, northern Italy), Quaternary Res.,
605 83, 324-335, https://doi.org/10.1016/j.yqres.2014.12.005, 2015.

Ladanyi, B.: Rheology of ice/rock systems and interfaces, The Eighth International Conference on Permafrost, Zurich, Switzerland, 2003, WOS:000185049300110, 621-626,

Leopold, M., Williams, M. W., Caine, N., Völkel, J., and Dethier, D.: Internal structure of the Green Lake 5 rock glacier, Colorado Front Range, USA, Permafrost Periglac., 22, 107-119, https://doi.org/10.1002/ppp.706, 2011.

610 Mellor, M., and Testa, R.: Effect of temperature on the creep of ice, J. Glaciol., 8, 131-145, 1969.

Monnier, S., and Kinnard, C.: Internal structure and composition of a rock glacier in the Andes (upper Choapa valley, Chile) using borehole information and ground-penetrating radar, Ann. Glaciol., 54, 61-72, https://doi.org/10.3189/2013AoG64A107, 2013.

Monnier, S., and Kinnard, C.: Reconsidering the glacier to rock glacier transformation problem: New insights from the central Andes of Chile, Geomorphology, 238, 47-55, https://doi.org/10.1016/j.geomorph.2015.02.025, 2015a.

615   Monnier, S., and Kinnard, C.: Internal structure and composition of a rock glacier in the Dry Andes, Inferred from ground-penetrating radar data and its artefacts, Permafrost Periglac., 26, 335-346, https://doi.org/10.1002/ppp.1846, 2015b.

Monnier, S., and Kinnard, C.: Interrogating the time and processes of development of the Las Liebres rock glacier, central Chilean Andes, using a numerical flow model, Earth Surf Proc Land., 41, 1884-1893, 10.1002/esp.3956, 2016.

Moore, P. L.: Deformation of debris-ice mixtures, Rev. Gepphys., 52, 435-467, https://doi.org/10.1002/2014rg000453, 2014.

620   Munroe, J. S.: Distribution, evidence for internal ice, and possible hydrologic significance of rock glaciers in the Uinta Mountains, Utah, USA, Quaternary Res., 90, 50-65, https://doi.org/10.1017/qua.2018.24, 2018.

Nan, Z., Li, S., and Liu, Y.: Mean annual ground temperature distribution on the Tibetan plateau: Permafrost distribution mapping and further application, Journal of Glaciology and Geocryology, 24, 142-148, 2002.

Obu, J.; Westermann, S.; Barboux, C.; Bartsch, A.; Delaloye, R.; Grosse, G.; Heim, B.; Hugelius, G.; Irrgang, A.; Kääb, A.M.; Kroisleitner,
625   C.; Matthes, H.; Nitze, I.; Pellet, C.; Seifert, F.M.; Strozzi, T.; Wegmüller, U.; Wieczorek, M.; Wiesmann, A. (2020): ESA Permafrost Climate Change Initiative (Permafrost_cci): Permafrost version 2 data products. Centre for Environmental Data Analysis, *date of citation*. http://catalogue.ceda.ac.uk/uuid/1f88068e86304b0fbd34456115b6606f

Oerlemans, J.: Glaciers and climate change, A.A. Balkema Publishers, Lisse, 2001.

PERMOS: Permafrost in Switzerland 2014/2015 to 2017/2018, edited by: Noetzli, J., Luethi, R., and Staub, B., the Cryospheric Commission
630   of the Swiss Academy of Sciences, Glaciological Report (Permafrost) No. 12–15, 104 pp., 2019.

Rangecroft, S., Harrison, S., Anderson, K., Magrath, J., Castel, A. P., and Pacheco, P.: A first rock glacier inventory for the Bolivian Andes, Permafrost Periglac., 25, 333-343, https://doi.org/10.1002/ppp.1816, 2014.

Reznichenko, N., Davies, T., Shulmeister, J., and McSaveney, M.: Effects of debris on ice-surface melting rates: an experimental study, J. Glaciol., 56, 384-394, https://doi.org/10.3189/002214310792447725, 2010.

635   Salerno, F., Guyennon, N., Thakuri, S., Viviano, G., Romano, E., Vuillermoz, E., Cristofanelli, P., Stocchi, P., Agrillo, G., Ma, Y., and Tartari, G.: Weak precipitation, warm winters and springs impact glaciers of south slopes of Mt. Everest (central Himalaya) in the last 2 decades (1994–2013), The Cryosphere, 9, 1229-1247, https://doi.org/10.5194/tc-9-1229-2015, 2015.

Scott, W. J., Sellmann, P. V., and Hunter, J. A.: Geophysics in the study of permafrost, in: Geotechnical and Environmental Geophysics: Volume I, Review and Tutorial, 355-384, 1990.

640   Steig, E. J., Fitzpatrick, J. J., Potter, j. N., and Clark, D. H.: The geochemical record in rock glaciers, Geogr. Ann. A., 80, 277-286, https://doi.org/10.1111/j.0435-3676.1998.00043.x, 1998.

Vivian, R., and Bocquet, G.: Subglacial cavitation phenomena under the glacier D'Argentière, Mont Blanc, France, J. Glaciol., 12, 439-451, https://doi.org/10.3189/S0022143000031853, 1973.

Whalley, W. B., and Azizi, F.: Rheological models of active rock glaciers - evaluation, critique and a possible test, Permafrost Periglac., 5,
645   37-51, https://doi.org/10.1002/ppp.3430050105, 1994.

Zhao, L., and Sheng, Y.: Permafrost survey manual, Science Press, Beijing, 2015.